Journal of Power Sources 199 (2012) 322–330

Contents lists available at ScienceDirect

Journal of Power Sources

journal homepage: www.elsevier.com/locate/jpowsour

New insights into the limiting parameters of the Li/S rechargeable cell

Céline Barchasz[a,b,*], Jean-Claude Leprêtre[b], Fannie Alloin[b], Sébastien Patoux[a]

[a] French Atomic Energy and Alternative Energy Agency (CEA), Laboratory of Innovation for New Energy Technologies and Nanomaterials (LITEN), 17 rue des Martyrs, 38054 Grenoble Cedex 9, France
[b] Laboratoire d'Electrochimie et Physicochimie des Matériaux et Interfaces (LEPMI), UMR 5279, Grenoble INP - Université de Savoie - Université Joseph Fourier, 1130 rue de la Piscine, BP75, 38402 Saint Martin d'Hères, France

ARTICLE INFO

Article history:
Received 13 May 2011
Received in revised form 4 July 2011
Accepted 5 July 2011
Available online 18 July 2011

Keywords:
Rechargeable batteries
Lithium/sulfur
Sulfur pre-treatments
Electrochemical performance

ABSTRACT

The lithium/sulfur (Li/S) battery is a promising electrochemical system that has high theoretical capacity of 1675 mAh g^{-1}. However, the system suffers from several drawbacks: poor active material conductivity, active material dissolution, and use of the highly reactive lithium metal electrode. This study was aimed at understanding the most important limiting parameters of a Li/S cell. Different sulfur material pre-treatments were experimented to increase the practical capacity, and various morphologies were obtained. But none of these treatments led to improvements in electrochemical performance. Electrolyte additives were also used to increase cell discharge capacity, but again without success. Finally, it was concluded that the cell capacity limitation may be linked to dissolution of sulfur material and to passivation of the positive electrode. As the final discharge products are insulating and poorly soluble, they precipitate and induce passivation of the positive electrode surface, leading to incomplete active material utilization. EIS measurements confirmed this passivation problem.

1. Introduction

The development of rechargeable batteries is of considerable importance because of the increasing energy consumption of portable devices. Lithium-ion batteries have been under intense research over the past 20 years due to their advantages, such as high energy density, high operating voltage and low self-discharge [1]. Lithium transition-metal oxides, especially $LiCoO_2$ and its counterparts, are currently dominating the commercial lithium-ion battery market. However, the gravimetric energy density is known to be limited to 200–250 Wh kg^{-1}, which is not sufficient to meet electric vehicle battery requirements for extended ranges. Moreover, cobalt is toxic and expensive, and layered oxides usually have safety issues [2].

Elemental sulfur is a promising positive electrode material for lithium batteries due to its high theoretical specific capacity of about 1675 mAh g^{-1}, much greater than the 100–250 mAh g^{-1} attainable with the conventional lithium-ion positive electrode materials [3]. The average discharge potential is around 2.1 V (*vs.* Li^+/Li) and the complete Li/S system should allow a gravimetric energy density close to 500 Wh kg^{-1} to be reached. In addition, elemental sulfur is readily available and non-toxic, advantages that should enable cheap and safe high-energy batteries to be produced [4]. All the above-mentioned key parameters help explain the increasing number of publications on this topic.

Sulfur reduction is a multistep electrochemical process that can involve different intermediate species [5,6]. Lithium metal reacts with elemental sulfur (S_8) to produce lithium polysulfides with a general formula Li_2S_n. The first polysulfides that are produced, such as Li_2S_8 and Li_2S_6, have a long chain length. During discharge, the polysulfide chain length is shortened as the sulfur is further reduced. At the end of discharge, the final product is lithium sulfide (Li_2S) and the overall reaction equation is [7]:

$$16Li + S_8 \rightarrow 8Li_2S$$

This technology has attracted the attention of the electrochemistry community for many years [4,8]. However, it still suffers from several drawbacks. Indeed, sulfur and lithium sulfide are highly insulating materials [9,10] and the positive electrode must contain a significant and well-dispersed amount of electronic conductor, such as carbon or metal. Sulfur and lithium polysulfides are also soluble in common organic liquid electrolytes [11]. They can spontaneously diffuse through the liquid electrolyte, thus leading to lithium metal corrosion and self-discharge, in parallel with an increase in the electrolyte viscosity [12,13]. Once dissolved in the electrolyte, they can also react at the negative electrode, leading to a shuttle mechanism that delays the end of charge and drastically decreases coulombic efficiency [12,13]. On the other hand, the fully reduced compound, Li_2S, is insoluble, insulating, and may passivate the surface of both positive and negative electrodes [14–16].

* Corresponding author. Tel.: +33 438 78 91 62; fax: +33 438 78 51 98.
E-mail address: celine.barchasz@cea.fr (C. Barchasz).

0378-7753/$ – see front matter © 2011 Elsevier B.V. All rights reserved.
doi:10.1016/j.jpowsour.2011.07.021

For these reasons, sulfur utilization and cycle life are usually very low. Finally, the use of a lithium metal negative electrode is known to be a problem in large-scale utilization, since it may lead to short-circuits induced by dendrite formation and explosions.

The literature reports different strategies that have been considered to improve Li/S cell electrochemical performance. On the cathode side, carbon/sulfur composites can be designed so as to trap sulfur and lithium polysulfides [17,18]. The use of mesoporous or nanostructured carbon materials helps to decrease the shuttle mechanism as well as self-discharge by preventing sulfur material diffusion through the electrolyte. The authors report a high discharge capacity along with an improved cycle life. However, they finally agree that lithium polysulfides may diffuse at some moment [17,18], whatever is done to the positive electrode morphology and/or composition. Another strategy involves optimizing the liquid electrolyte composition and many studies have been carried out on this subject. The discharge capacity can be increased thanks to the use of an ether-based optimized electrolyte composition [19–21]. Some additives can also improve battery performance [22]. For example, it was recently found that lithium nitrate can be a successful additive, leading to coulombic efficiency of close to 100%. It is assumed that this chemical product decomposes on the lithium metal anode, leading to good lithium metal passivation and avoiding further reaction with lithium polysulfides [8,23]. Another promising strategy is to use polymer electrolytes such as polyethylene oxide-based ones. These polymer electrolytes delay diffusion of the lithium polysulfides and sulfur dissolution, leading to decreasing self-discharge [24,25]. Various studies have also been carried out on protection of the metallic lithium negative electrode [26,27]. This strategy is aimed at preventing contact between the dissolved lithium polysulfides and the highly reactive lithium electrode by using interlayers of polymer or ceramic materials.

Bearing in mind all these strategies, our work was aimed at understanding some of the important limiting parameters of this Li/S system. We set out to determine the most relevant parameters that should be considered in order to improve the electrochemical performance of the Li/S cell. More precisely, we focused on the positive electrode side, trying to obtain different sulfur materials and cathode morphologies thanks to various pre-treatments, in order to extend both capacity and cycle life.

2. Experimental

Sulfur pre-treatments – Refined sulfur (−100 mesh, Aldrich) was used as the reference active material source. Sieved sulfur (−325 mesh, 99.5%) was also purchased from Alfa Aesar. Different sulfur pre-treatments were performed on the reference active material in order to obtain different sulfur morphologies. Sulfur was first ball-milled (dry or in hexane, planetary ball-mill, Retsch PM200, 50 mL stainless-steel jar, and three Ø20 mm diameter stainless steel balls) so as to decrease the particle size. Sulfur material was also ball-milled under the same conditions (dry ball-milling) with carbon black (Super P®, Timcal, S/C ratio of 10/90 wt%). A thermal treatment was finally performed on the sulfur material, the idea being to change the particle morphology.

Positive electrode preparation – Bare or pre-treated sulfur materials were then mixed with poly(vinylidene fluoride) (PVdF 1015, dissolved in N-methyl-2-pyrrolidinone (12 wt%), Solvay), carbon black (Super P®, Timcal) and mixed in N-methyl-2-pyrrolidinone (NMP, anhydrous, 99.5%, Aldrich). The S/C/binder mixing ratio was generally 80/10/10 wt%. But we also investigated the impact of carbon content, ranging from 10 to 45 wt%, decreasing the sulfur content while keeping 10 wt% of binder. After homogenization, the slurry was coated onto a 20 μm thick aluminum current collector by doctor blade technique. The resulting cathodes were dried at 55 °C for 24 h, then cut into Ø14 mm disks and finally dried for 24 h under vacuum at room temperature. The coating thickness was about 100 μm so as to obtain a 20 μm thick cathode after drying. The positive electrode area was 1.539 cm^2. The cathode compositions are summarized in Table 1.

2-Electrode cell assembly – The positive electrodes, described in Table 1, were assembled in an argon-filled glovebox in 2032 coin cells. Lithium metal foil was used as a negative electrode and Celgard 2400® as a separator. A non-woven Viledon® separator (polypropylene-based membrane) foil was also added between the cathode foil and the Celgard® to store a large amount of electrolyte on the cathode side. A liquid electrolyte was prepared by mixing tetraethylene glycol dimethyl ether (TEGDME, 99%, Aldrich) and 1,3-dioxolane (DIOX, anhydrous, 99.8%, Aldrich) with a volume ratio of 50/50. Lithium bis(trifluoromethane sulfone)imide (LiTFSI, 99.95%, Aldrich) was used as a lithium salt and was dissolved at 1 mol L^{-1} in the mixed solvents. About 150 μL of electrolyte were then added to the coin cell to fully wet both electrodes and separators.

3-Electrode cell assembly – The positive electrode was also assembled in an argon-filled glovebox in 3-electrode 2032 coin cells. The cells were assembled as previously described except that a second lithium metal electrode was inserted between the Viledon® and the Celgard® separators. This third electrode was wrapped in Kapton® beforehand. A schematic diagram of a 3-electrode coin cell is presented in Fig. 1.

Characterization techniques – The structure and morphology of pre-treated sulfur samples were analyzed by X-ray Diffraction (XRD, Brüker D8000 diffractometer, Cu Kα radiation) and Scanning Electron Microscopy (SEM, Philips XL30). Particle size analyses (Malvern MasterSizerS) and specific surface area analyses (BET method, Micromeritics, Tristar II 3020) were also performed. Electrochemical tests were monitored on 2-electrode cells with an Arbin battery cycler between 1.5 and 3.0 V (*vs.* Li^+/Li) at room temperature and a cycling rate of C/10. Electrochemical Impedance Spectroscopy (EIS) measurements were carried out on the 3-electrode cells with a VMP2 potentiostat (Bio-logic, Claix) within the 200,000–0.001 Hz range and with a 5 mV amplitude.

Table 1
Summary of cathode compositions.

Name	Sulfur source	Pre-treatment	Final S/C/PVDF ratio/wt%	Theoretical capacity/mAh cm^{-2}
Ref	Refined	None	80/10/10	3.3
C1	−325 mesh	None	80/10/10	2.7
C2	Refined	Dry ball-milling	80/10/10	3.3
C3	Refined	Ball-milling in hexane	80/10/10	3
C4	Refined	Thermal treatment	80/10/10	2.5
C5	Refined	Ball-milling with carbon	70/20/10	1.5
C6	Refined	None	70/20/10	1.7
C7	Refined	None	60/30/10	1.4
C8	Refined	None	45/45/10	0.7

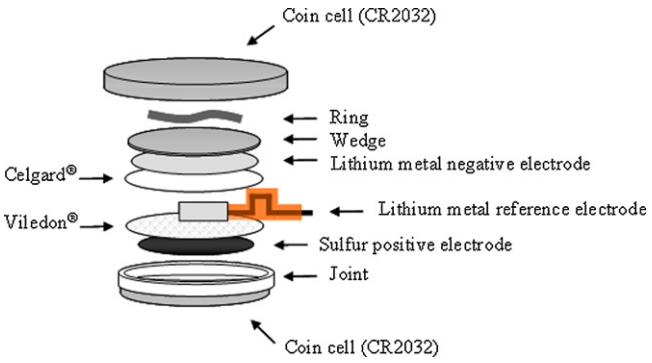

Fig. 1. Schematic diagram of a 3-electrode coin cell.

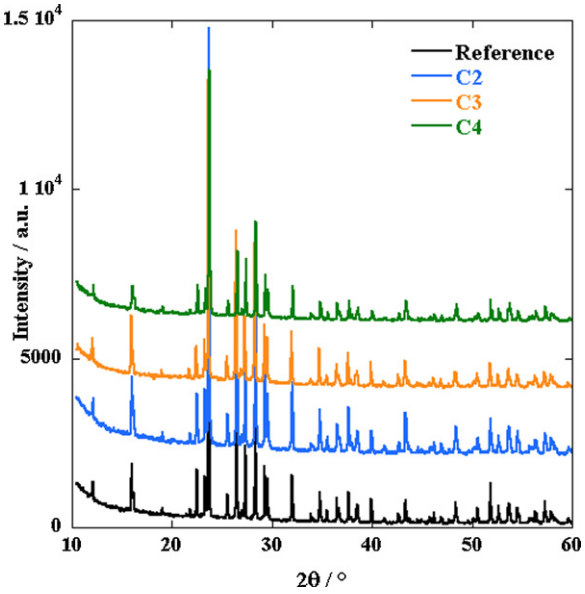

Fig. 2. XRD patterns of the pre-treated sulfur materials.

3. Results and discussion

Characterization of materials – The XRD patterns of pre-treated sulfur materials are presented in Fig. 2. They indicate that the sulfur crystalline phase did not change with pre-treatments. The α-orthorhombic phase remained the most stable phase even for the thermally treated sample. On the other hand, the sample morphology changed significantly with pre-treatments. SEM images and particle size distributions are presented in Figs. 3 and 4 respectively. They both show that the sulfur material had two different grain sizes: the dispersed grains are the primary particles that form larger particles when aggregating, designated as secondary particles. The BET measurements are summarized in Table 2. Bare sulfur consisted of ovoid-shaped particles with an average grain size of 34 μm. The dry ball-milling resulted in particles aggregation, since elemental sulfur material tends to stick. The average grain size increased from 34 μm to 60 μm. Ball-milling in hexane led to a dras-

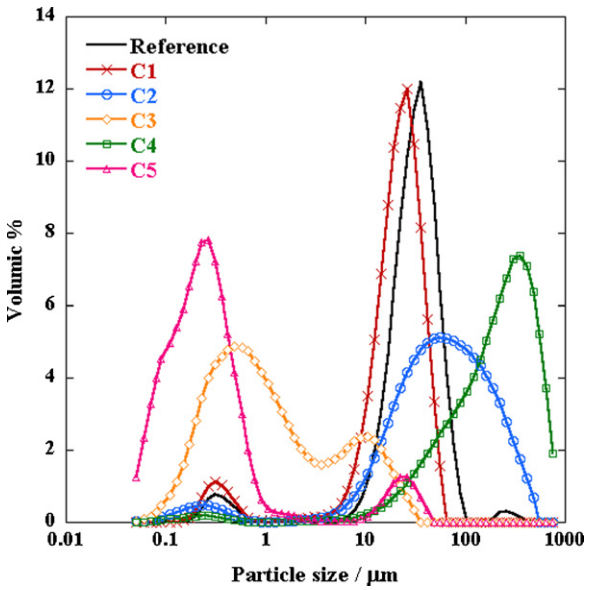

Fig. 4. Particle size distribution of the pre-treated sulfur materials.

Table 2
Average particle sizes and BET measurements of the pre-treated sulfur materials.

Name	Sulfur source	Average particle size/μm	BET/$m^2\ g^{-1}$
Ref	Bare sulfur	34	<0.01
C1	Sieved sulfur	20	0.14
C2	Dry ball-milling	60	<0.01
C3	Ball-milling in hexane	0.92	3
C4	Thermal treatment	200	0.1
C5	Ball-milling with carbon	0.25	0.9

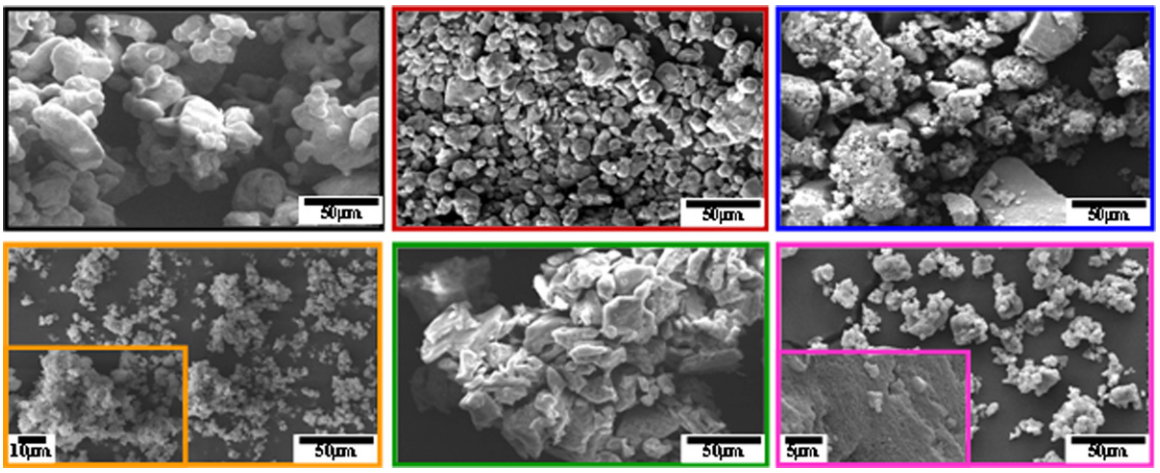

Fig. 3. SEM images of the pre-treated sulfur materials.

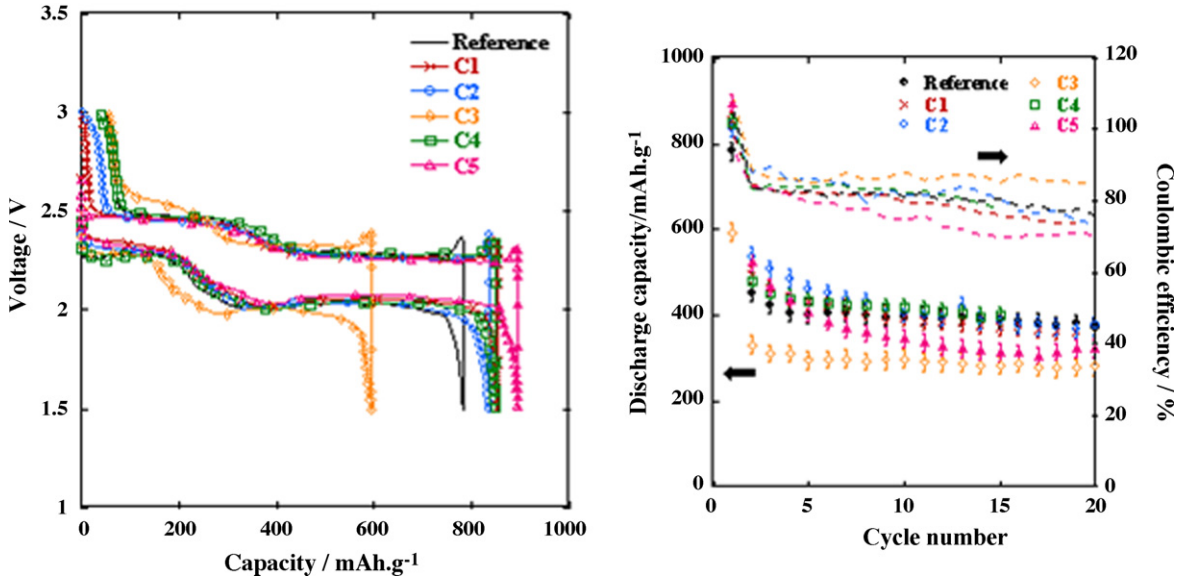

Fig. 5. First cycle profile, capacity fading and coulombic efficiency of the different cathode materials. The capacities are given in mAh g^{-1} of sulfur material contained in the positive electrode.

tic decrease in grain size, to below 1 μm. While the surface area of the bare sulfur particles was quite small (below the detection limit of 0.01 $m^2\ g^{-1}$), the surface area of this wet-milled sulfur increased to 3 $m^2\ g^{-1}$. Thermal treatment led to a decrease in primary particle size, as revealed by BET measurements, while the secondary particle size increased to about 100 μm. This porous structure can be filled with carbon material, which is then well-dispersed into the porous sulfur matrix, providing a more conductive composite material. As a result, the overall conductivity of the electrode can be increased. Finally, a carbon coating was applied to the sulfur particles by dry ball-milling with carbon. This pre-treatment did not have a significant effect on the sulfur grain size, as evidenced by the grain size distribution. The 0.1–1 μm distribution is mainly due to the non-aggregated Super P® carbon material rather than to the sulfur nanomaterial. The image offset clearly shows the carbon aggregation onto the micron-sized sulfur particles, thereby possibly protecting active material particles from the electrolyte.

Electrochemical characterization of 2-electrode cells – The first cycle profile and capacity fading of the different cathode materials are presented in Fig. 5. Ball-milling in hexane (C3 sample) was surprisingly detrimental for the cell electrochemical performance, the discharge capacity being far lower than for the other cases. This could be explained by the increased specific surface area of active material particles, leading to enhanced sulfur/electrolyte contact. Sulfur quickly dissolves in the electrolyte, even just after cell assembly, chemically reacting with metallic lithium and leading to a significant self-discharge process.

As regards the other pre-treatments, the expected effects were not obtained, with the first discharge capacity and cycle life hardly modified. All first discharge capacities remained close to 850 mAh g^{-1}. These results suggest that these pre-treatments might not help to improve cell electrochemical performance. During the first discharge, sulfur material was reduced and formed soluble lithium polysulfides compounds. As a consequence of this dissolution, the carbon coating may be ineffective after the first discharge periods. In the case of thermal treatment (C4 sample), the porous structure might help to improve carbon black dispersion and thus the electronic conductivity of the electrode. But this did not improve electrochemical performance. As a result, and mainly because of dissolution, the electronic conductivity of the composite cathode may not be a relevant parameter to work on. Indeed, in this study, the cycling rate was rather low, *i.e.* C/10, and the discharge capacity was not expected to be limited by the electronic conductivity of the cathode. The limiting parameter may instead be linked to the dissolution process and/or to the loss of active material, which diffuses through the electrolyte and then reacts on the lithium metal electrode. Since the dissolution process occurs during the first steps of discharge, optimization of the positive electrode might have very little impact on performance enhancement. Finally, Fig. 5 also highlights the poor coulombic efficiency of about 80% obtained for Li/S cells. This indicates that the shuttle mechanism occurred partially during the charge process, also indicating that dissolved lithium polysulfides reacted easily with lithium metal.

In an effort to increase the sulfur content and the discharge capacity of the coin cell, an additional sulfur source was added to the reference electrolyte. Lithium polysulfides were synthesized by mixing an appropriate amount of elemental sulfur and lithium metal in TEGDME so as to reach a 1 mol L^{-1} concentration equivalent Li_2S_6. After stirring for 48 h, all products were dissolved, giving a dark brown, viscous solution. The final composition of this polysulfide-containing electrolyte was LiTFSI 1 mol L^{-1} + equivalent Li_2S_6 0.1 mol L^{-1} + TEGDME/DIOX 50/50 vol%. Firstly, this test was aimed at increasing the amount of sulfur that might be subject to reduction by unit of electrode area. This extra capacity may help to improve the resulting capacity. A further goal was to add some extra polysulfide species to test their ability to passivate the lithium metal interface, without losing any active material from the positive electrode. The aim was to determine whether this passivation reaction would help improve both discharge capacity and fading. The first cycle profile and capacity fading are presented in Fig. 6, and compared to the reference test. Both cells (with and without addition of Li_2S_6 in the electrolyte) delivered about 900 mAh g^{-1}, and retained only 60% of the initial capacity after 10 cycles. This extra capacity did not therefore appear to have helped increase the capacity or the cycle life. The passivation provided by these extra polysulfides did not help to further decrease the lithium metal/sulfur active material reaction. The coulombic efficiency was even reduced in comparison with the additive-free electrolyte, and the shuttle mechanism is clearly visible on the first cycle.

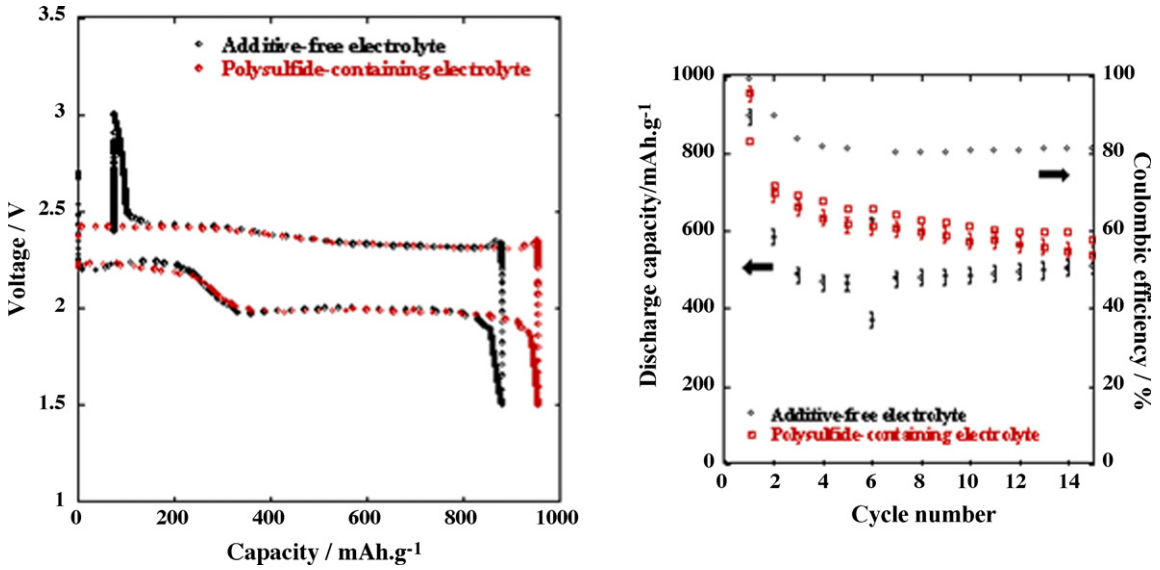

Fig. 6. First cycle profile, capacity fading and coulombic efficiency of cells containing additive-free and polysulfides-based electrolytes. The capacities are given in mAh g^{-1} of sulfur material contained in the positive electrode.

Lithium nitrate was used as an electrolyte additive, since it is reported in the literature to be a powerful additive for achieving good passivation of the lithium metal electrode surface [8,23]. We investigated whether this protective additive would prevent the polysulfide compounds from reacting with lithium metal during cycling. The electrolyte was prepared by adding lithium nitrate ($LiNO_3$, 99.99%, Aldrich) to the reference electrolyte so as to reach a $LiNO_3$ final concentration of 0.1 mol L^{-1}. The cycle life of the cell containing $LiNO_3$-based electrolyte is presented in Fig. 7, and compared with the reference one. Coulombic efficiency was significantly enhanced by using this additive, meaning that the polysulfide/lithium reaction and/or shuttle mechanism were decreased. On the other hand, since capacity fading was not affected, this indicates that this efficient lithium metal passivation did not impact on capacity decay.

The electrochemical tests thus indicated that:

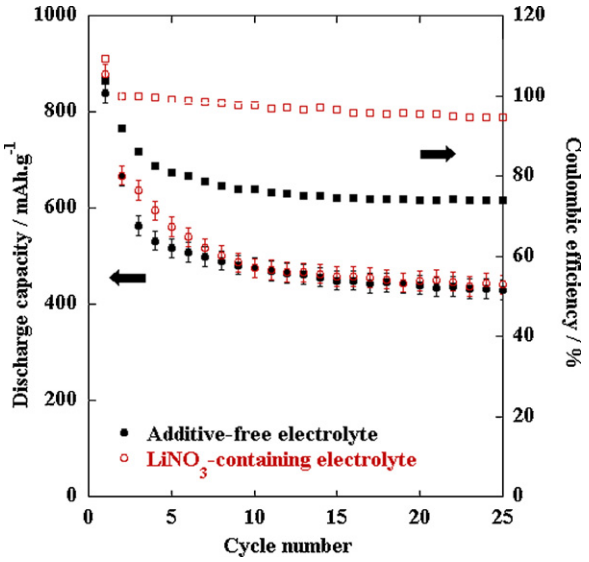

Fig. 7. Cycle life of reference electrode with additive-free and $LiNO_3$-containing electrolytes. The capacities are given in mAh g^{-1} of sulfur material contained in the positive electrode.

- Working on the active material morphology did not enable the theoretical sulfur capacity to be reached.
- Increasing the cell sulfur content (with a constant electrode surface) did not help to increase the practical discharge capacity.
- Carrying out efficient lithium metal passivation did not prevent capacity fading and had only a minor effect on the practical discharge capacity.

As reported in the literature [14,15], the first discharge step is linked to sulfur dissolution and long polysulfide production. On the other hand, the end of discharge is linked to the formation of short polysulfides, compounds that are less soluble and insulating. These products are known to precipitate during the second discharge step, covering the positive electrode surface [14,15]. In fact, the capacity limitation may be linked to the passivation of the positive electrode, with discharge stopping when the surface is fully covered by these insulating species. This assumption is in agreement with the fact that pre-treatments did not help to improve the practical capacity. Because of the sulfur dissolution during discharge, the resulting electrode surface area is not associated with the starting cathode morphology. This also conveniently explains why the polysulfide-based electrolyte did not improve practical capacity: discharge stopped because of electrode passivation and not because of a lack of active species. Finally, this fact would explain why efficient lithium metal passivation did not help the theoretical sulfur capacity to be reached: the active material was still present on the cathode side but could not be further reduced due to electrode passivation. Then, it might be suggested that surface area (and thus the carbon amount) could impact the overall performance of the system.

Indeed, Fig. 8 shows a big improvement in cell capacity with the increase in carbon content. To analyze this improvement, the discharge capacity was plotted versus the sulfur electrode percentage, as presented in Fig. 9. A linear evolution can be observed, *i.e.* the capacity decreases linearly when the sulfur amount is increased. Furthermore, the extrapolation of this evolution almost reaches the theoretical sulfur capacity of 1675 mAh g^{-1} (1590 mAh g^{-1} for the calculated parameter), when the active material content tends towards zero. The decreasing sulfur amount leads directly to an increase in the carbon material, with two effects (i) improved electrode electronic conductivity, and (ii) an increase in the resulting electrode surface area after sulfur dissolution.

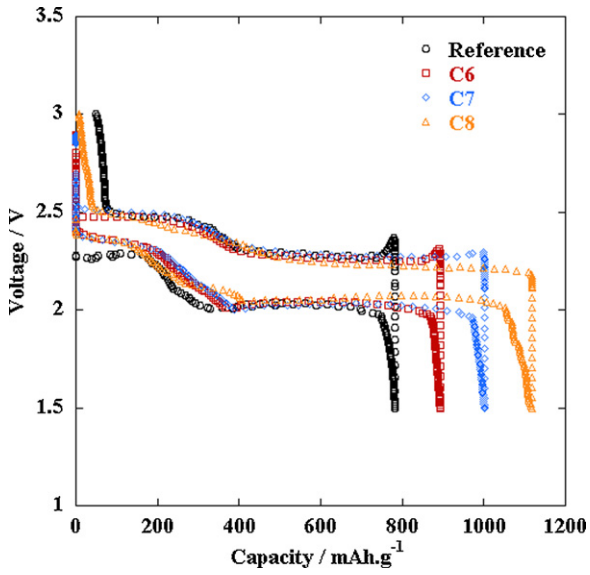

Fig. 8. Charge and discharge profile of Li/S cells with a varying carbon content. The capacities are given in mAh g^{-1} of sulfur material contained in the positive electrode. The charge voltage profile starts with a potential drop that could be linked to the passivation layer dissolution. This drop decreases as the conductive carbon content increases, indicating that the blocking interface may also be decreased. In addition, the discharge capacity seems to increase linearly with the conductive additive amount.

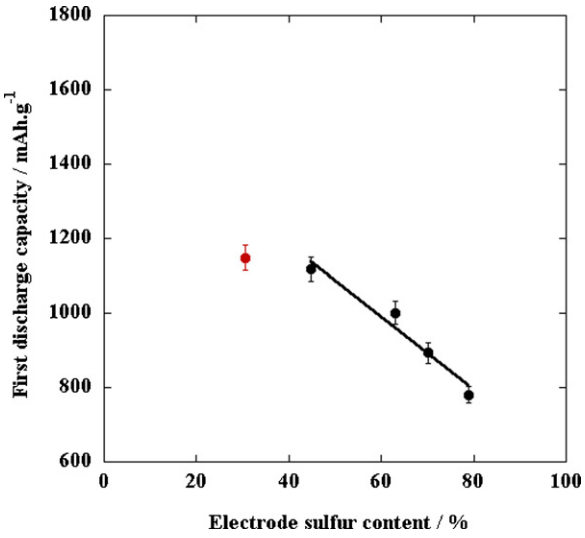

Fig. 9. Discharge capacity versus sulfur content in positive electrodes, with a constant binder percentage of 10 wt%.

The linear increase in capacity with the amount of carbon cannot be explained by electronic conductivity limitation, since the evolution should not be linear due to the percolating effect. On the other hand, the linear evolution can be linked to the increasing electrode surface area, in accordance with the fact that the capacity could be limited by the complete electrode passivation at the end of discharge, as previously suggested.

From a theoretical point of view, we can say that if a small amount of sulfur is used in the electrode, the entire material content should be active and the theoretical capacity should be reached. The surface area would then no longer be a limiting parameter. However, this was not the case in practice, and the capacity obtained for a low sulfur amount, *i.e.* 30%, no longer evolved linearly (1150 mAh g^{-1} instead of the calculated value, *i.e.* 1280 mAh g^{-1}). This can be explained by the loss of active material, which may be involved in parasite reactions, as for example in the negative electrode passivation. With high sulfur amount, this irreversible loss can be considered negligible as regards the whole sulfur content, which was no longer the case with low content.

The amount of carbon also had an impact on the overpotentials observed at the start of charge (Fig. 8). Indeed, when the carbon content is increased, we can assume that the electrode surface area is also increased, and that the passivation film formed at the end of discharge is thinner. Indeed, because of the larger amount of conductive additive, electrode conductivity must be higher and the resulting overpotentials would decline.

Discharge capacity thus appears to be governed by (i) positive electrode surface and (ii) lithium polysulfide solubility linked to the electrolyte composition. Indeed, the cathode surface area dictates the amount of insulating species that can be deposited at the end of discharge. A high surface area would lead to a delay in the passivation of the whole electrode surface, thus delaying the end of discharge. The positive electrode should also keep its structure during cycling and thus reduce capacity fading. As regards electrolyte composition, it controls short polysulfide solubility, consequently contributing to the delay in species precipitation.

Capacity fading could thus be linked to dissolution/precipitation cycles, which lead to cathode pulverization. A cycled sulfur electrode is presented in Fig. 10, and compared with a non-cycled one. The SEM images indicate that the initial morphology was profoundly modified during cycling. Indeed, starting with elemental sulfur, the active material dissolves in the electrolyte at the beginning of discharge, and converts into soluble lithium polysulfides. At this point, the composite electrode may essentially be composed of carbon nanomaterial and binder. As sulfur material has micron-sized particles, and accounts for 80 wt% in the mass of the electrode, its dissolution may lead to a highly porous structure formation. In addition, loss of carbon material may occur in the electrolyte. Both processes explain the modification of the electrode morphology

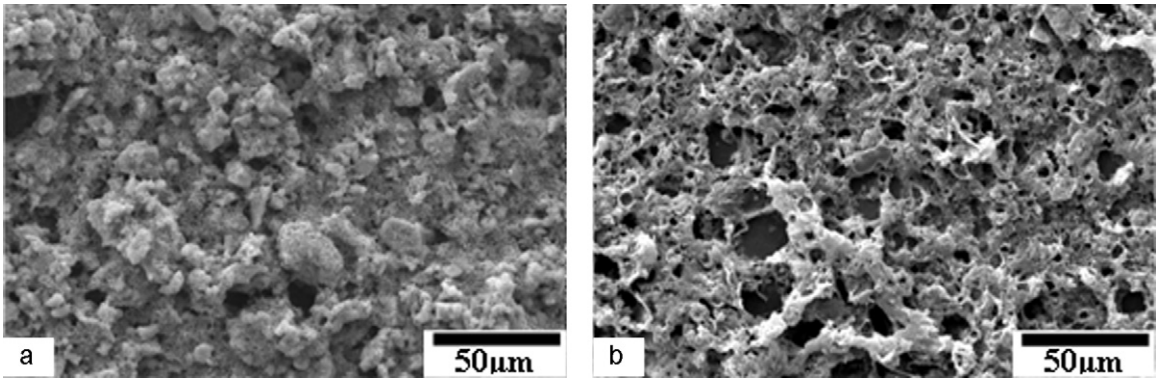

Fig. 10. SEM pictures of a sulfur positive electrode: a – before cycling/b – after one cycle.

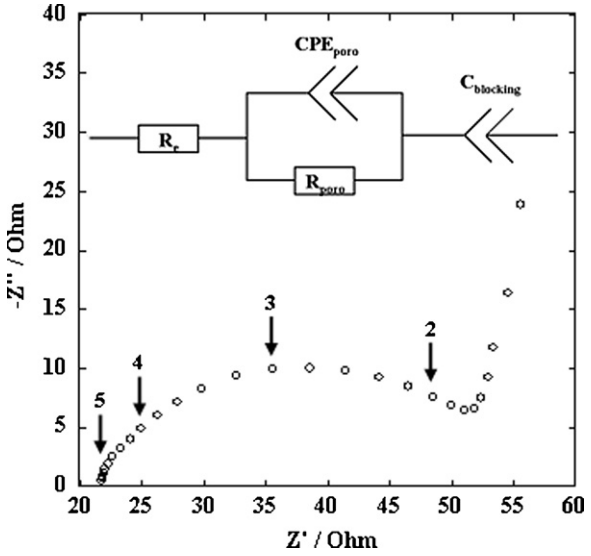

Fig. 11. Nyquist plot of reference positive electrode obtained before cycling. Offset: possible equivalent circuit.

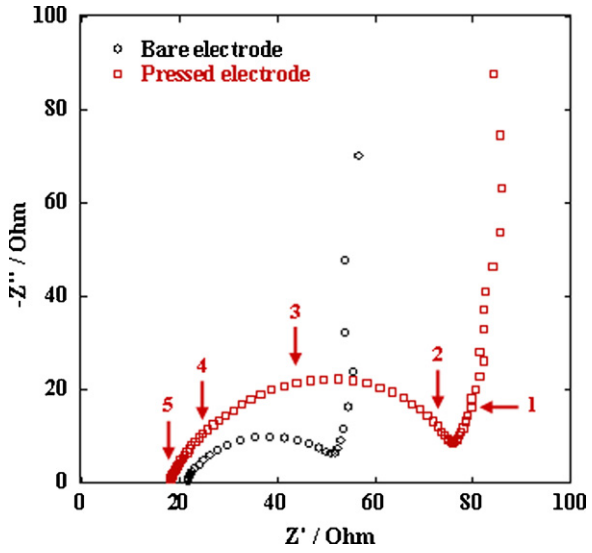

Fig. 12. Nyquist plots obtained before cycling for a bare sulfur positive electrode and a pressed one (0.65 t cm^{-2}).

along the discharge process. Moreover, since some of the carbon conductor material may be detached from the current collector, one can suggest that the resulting positive electrode surface area may be reduced and then the specific capacity.

Electrochemical characterization of 3-electrode cells – EIS measurements were performed on 3-electrode cells during cycling to investigate positive electrode behavior. The common Nyquist plot obtained for the reference positive electrode before cycling is presented in Fig. 11. The frequency is given in a logarithmic scale on the graph. The impedance spectrum shows a high frequency (HF) flat semi-circle and a low frequency (LF) straight line, which represents the blocking character of the non-lithiated electrode, schematized by a pure capacitance $C_{blocking}$. The very high frequency (VHF) response is linked to electrolyte and contact resistances, as generally agreed [28]. This can be schematized by a pure resistance R_e. The HF semi-circle might not be linked to the formation of a solid electrolyte interface (SEI), since Li/S open-cell potential is around 2.5–2.7 V (*vs.* Li^+/Li). Indeed, at this potential, the electrolyte is electrochemically stable and a passivation layer would not be expected to form on the sulfur electrode. On the other hand, it has previously been mentioned that porous electrodes, such as graphite electrodes, show an additional HF semi-circle that may not relate to a passivation layer, but rather to contact problems occurring between different phases or different particles inside the electrode, as well as porosity effects [28]. The equivalent circuit associated with this HF semi-circle is R_{HF}//CPE_{HF} (Constant Phase Element). Indeed, it seems more appropriate to use one R//CPE circuit rather than several R//C circuits in series. The Constant Phase Element translates in an empirical manner, the non-ideal behavior of the composite electrode (porosity of the material, roughness of the surface). The likely equivalent circuit is presented in Fig. 11 offset.

The positive electrode composite material was composed of sulfur particles, carbon conductive agent particles and binder. The cathode was therefore relatively porous (close to 60% porosity). Thus it was assumed that the HF semi-circle might be linked to both ionic mobility of the electrolyte inside the sulfur electrode pores and/or to contact problems. In order to achieve the HF semi-circle attribution, the positive electrode was pressed at 0.65 t cm^{-2}. This compression induced a decrease in the electrode porosity from 60% to 33%. The corresponding impedance spectra are presented in Fig. 12. A large increase in the HF semi-circle resistance can be observed, while the pseudo-capacity values remain of the same order of magnitude for the bare and pressed electrodes. The porosity decrease could have two effects: improvement of electrical contacts and decrease in both pore size and the amount of open porosity. Electrical contact improvement should result in a decrease in the resistance value. However, as the opposite was observed, the HF semi-circle could not be related to poor contacts and seemed to be related to the ionic mobility of the electrolyte inside the sulfur electrode pores. Indeed, ion mobility resistance is directly related to tortuosity. A decrease in porosity leads to an increase in tortuosity and in the resulting resistance. We therefore concluded that the HF semi-circle was most likely to be related to ion mobility inside the electrode pores.

The impedance spectra of a sulfur electrode often show a loop at medium frequencies (MF), as is clearly visible in Fig. 13. A loop can be linked to inductive effects or to the non-stationary state

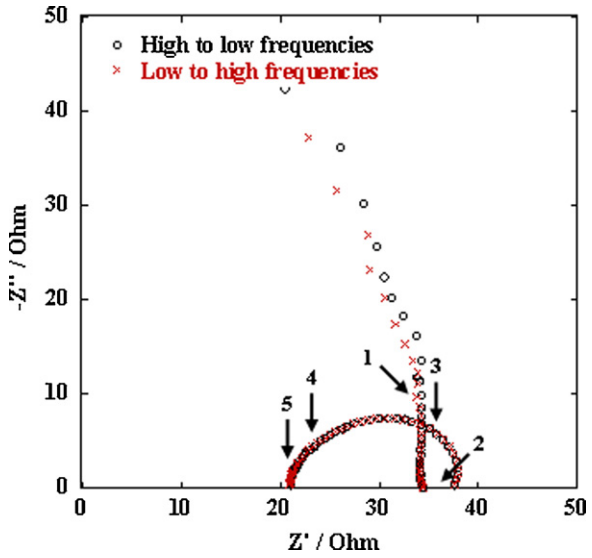

Fig. 13. Nyquist plot of reference positive electrode before cycling showing the commonly visible MF loop. EIS measurements were carried in two different ways: first from high to low frequencies, then from low to high frequencies. Changing the frequency sweep mode was intended to prevent instability effects that may occur for low frequency measurements.

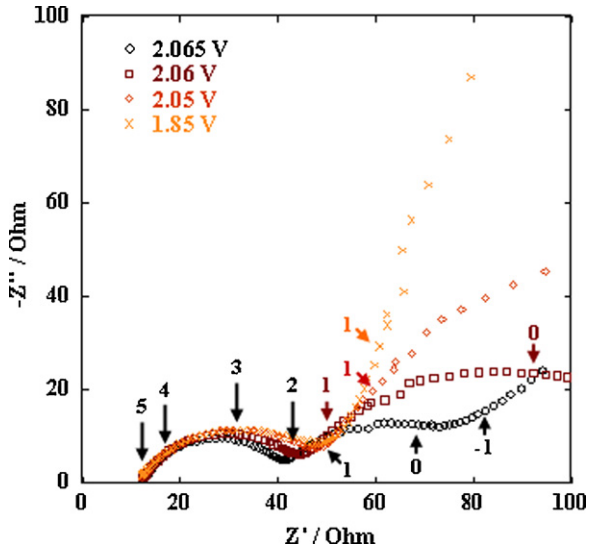

Fig. 14. Nyquist plots of reference positive electrode obtained for different states of discharge.

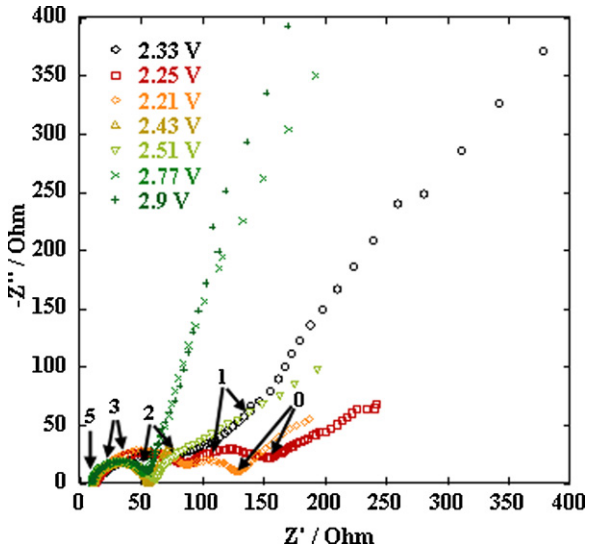

Fig. 15. Nyquist plots of reference positive electrode obtained for different states of charge. The potentials first decrease because of the potential drop occurring during the first moments of charge.

of the experimental system during measurements. The contact impedance (electric wiring) can behave like an inductive component, leading to loop formation. However, this kind of effect is observed at VHF. An inductive component at MF might be related to the presence of adsorbed species on the electrode surface, involved in the charge transfer reaction [29–31].

In order to make sure that EIS measurements were performed in the stationary state, the frequency sweep mode was changed. The frequency sweep was first performed in the HF to LF range, then in reverse, and the corresponding results are presented in Fig. 13. The reverse frequency scan entirely fits the first scan, meaning that this loop could not be linked to artefact effects, but rather to the presence of adsorbed species. The positive electrode discharge mechanism involves sulfur solubilization and the production of soluble long polysulfides. EIS measurements could induce some surface electrochemical reactions, leading to polysulfides formation. These products could possibly be adsorbed on the positive electrode surface, leading to the appearance of a MF loop.

EIS measurements were performed on the positive electrode during cycling. The impedance spectra obtained at different states of discharge are presented in Fig. 14. The HF semi-circle resistance increases slightly between 2.065 V and 1.85 V (*vs.* Li^+/Li). During discharge, sulfur consumption should induce a modification in the positive electrode morphology, which may explain the HF semi-circle evolution. At the beginning of discharge, a new semi-circle emerged in the MF range, largely dependent on the state of discharge. The latter can be linked to the charge transfer reaction, as commonly agreed in the literature [28,32]. The charge transfer resistance was the weakest at half-discharge. Indeed, at this potential, the electrochemical reaction concerns mobile soluble polysulfides, indicating that the transfer reaction kinetics are not limited by species diffusion. During the second discharge plateau, at 2.06 V (*vs.* Li^+/Li), an increase in charge transfer resistance can be observed. This could be related to a slower electrochemical reaction involving less soluble lithium polysulfides. At the end of discharge (1.85 V *vs.* Li^+/Li), the semi-circle is replaced by a straight line, indicating the electrode blocking character. This behavior is in agreement with the presence, at the end of discharge, of short polysulfides which are poorly soluble and insulating. Precipitation of these products could lead to the formation of a blocking layer on the positive electrode. When the surface is fully covered by this layer, the cell potential suddenly drops and the electrode behaves as a blocking interface. In fact, the EIS measurements support the fact that the discharge capacity may be limited by passivation of the positive electrode, as previously suggested. The presence of this passivation layer could thus induce an increase of the MF semi-circle resistance, as observed in Fig. 14.

EIS measurements were also performed on the positive electrode during the charge process. The corresponding plots are presented in Fig. 15. At the initial stage, the potential increased quickly, but then decreased, suggesting that the cell overpotential may be reduced, as presented in Fig. 8. This behavior is in agreement with the probable presence of a passive layer covering the cathode at the end of discharge. The current may oxidize the insulating polysulfides present at the electrode surface, which may be turned into more soluble species, leading to easier oxidation reactions. During charge, the HF semi-circle resistance decreased, which might be explained by changes in the electrode morphology and dissolution of the passive layer. The evolution is more significant than that observed during discharge. However, the resistance value obtained at the end of charge was close to the value obtained at the beginning of discharge.

The MF semi-circle resistance first dropped at the beginning of charge (ranging from 2.33 to 2.43 V *vs.* Li^+/Li) indicating that the charge transfer reaction became faster and faster. This is in agreement with the changes in the charge transfer resistance that could be observed during discharge. Thus, this evolution can be explained in the same way: the weakest resistance was obtained for half-charge (*i.e.* 2.43 V *vs.* Li^+/Li), when all the insulating compounds had been oxidized and dissolved in the electrolyte. The MF semi-circle resistance increased at the end of charge (ranging from 2.43 to 2.9 V *vs.* Li^+/Li). Indeed, the final product is insoluble and insulating elemental sulfur that might passivate the positive electrode when deposited during the charge process. Once again, the end of cycling occurs when the electrode surface is fully blocked, and the cell potential suddenly rises.

4. Conclusion

This study was aimed at understanding the most relevant parameters that may dictate Li/S cell electrochemical performance. EIS measurements and galvanostatic tests highlighted some key issues. Surprisingly, efficient metallic lithium passivation did not

help to increase discharge capacity or decrease capacity fading. However, it allowed coulombic efficiency of almost 100% to be reached. The sulfur pre-treatments reported in this paper had no impact on electrochemical performance due to rapid dissolution of active material. Adding polysulfides to the electrolyte could theoretically help to boost cell capacity, but this was not experimentally helpful in the configurations we tested. The impact of carbon content on discharge capacity clearly showed the predominant effect of the electrode surface at the end of discharge. Capacity limitation must be linked to passivation of the positive electrode, since this latter is quickly covered by insoluble, insulating products such as Li_2S. As a result, Li/S system performance is highly likely to be governed mainly by the electrolyte composition and the cathode specific surface area. A high surface area should help delay passivation of the entire electrode surface and end of discharge. The positive electrode should also retain its morphology during cycling so as to decrease capacity fading. With respect to electrolyte composition, it controls the solubility of short polysulfides, consequently helping delay species precipitation.

Acknowledgement

The authors would like to acknowledge the CEA-INSTN for supporting part of this study (PhD funding awarded to Céline Barchasz).

References

[1] J.M. Tarascon, M. Armand, Nature 414 (2001) 359–367.
[2] M. Armand, J.M. Tarascon, Nature 451 (2008) 652–657.
[3] B.L. Ellis, K.T. Lee, L.F. Nazar, Chem. Mater. 22 (2010) 691–714.
[4] R.D. Rauh, K.M. Abraham, G.F. Pearson, J.K. Surprenant, S.B. Brummer, J. Electrochem. Soc. 126 (1979) 523–527.
[5] H. Yamin, J. Penciner, A. Gorenshtein, M. Elam, E. Peled, J. Power Sources 14 (1985) 129–134.
[6] H. Yamin, A. Gorenshtein, J. Penciner, Y. Sternberg, E. Peled, J. Electrochem. Soc. 135 (1988) 1045–1048.
[7] Y. Jung, S. Kim, Electrochem. Commun. 9 (2007) 249–254.
[8] D. Aurbach, E. Pollak, R. Elazari, G. Salitra, C.S. Kelley, J. Affinito, J. Electrochem. Soc. 156 (2009) A694–A702.
[9] E. Peled, Y. Sternberg, A. Gorenshtein, Y. Lavi, J. Electrochem. Soc. 136 (1989) 1621–1625.
[10] Y.J. Choi, Y.D. Chung, C.Y. Baek, K.W. Kim, H.J. Ahn, J.H. Ahn, J. Power Sources 184 (2008) 548–552.
[11] H. Yamin, E. Peled, J. Power Sources 9 (1983) 281–287.
[12] J. Shim, K.A. Striebel, E. Cairns, J. Electrochem. Soc. 149 (2002) A1321–A1325.
[13] Y.V. Mikhaylik, J.R. Akridge, J. Electrochem. Soc. 151 (2004) A1969–A1976.
[14] S.E. Cheon, K.S. Ko, J.H. Cho, S.W. Kim, E.Y. Chin, H.T. Kim, J. Electrochem. Soc. 150 (2003) A796–A799.
[15] S.E. Cheon, K.S. Ko, J.H. Cho, S.W. Kim, E.Y. Chin, H.T. Kim, J. Electrochem. Soc. 150 (2003) A800–A805.
[16] V.S. Kolosnitsyn, E.V. Karaseva, Russ. J. Electrochem. 44 (2008) 506–509.
[17] X. Ji, K.T. Lee, L.F. Nazar, Nat. Mater. 8 (2009) 500–506.
[18] C. Liang, N.J. Dudney, J.Y. Howe, Chem. Mater. 21 (2009) 4724–4730.
[19] J.W. Choi, J.K. Kim, G. Cheruvally, J.H. Ahn, H.J. Ahn, K.W. Kim, Electrochim. Acta 52 (2007) 2075–2082.
[20] W. Wang, Y. Wang, Y. Huang, C. Huang, Z. Yu, H. Zhang, A. Wang, K. Yuan, J. Appl. Electrochem. 40 (2010) 321–325.
[21] D.R. Chang, S.H. Lee, S.W. Kim, H.T. Kim, J. Power Sources 112 (2002) 452–460.
[22] J.W. Choi, G. Cheruvally, D.S. Kim, J.H. Ahn, K.W. Kim, H.J. Ahn, J. Power Sources 183 (2008) 441–445.
[23] Y. Mikhaylik, US Patent 2008/0193835 A1.
[24] J. Hassoun, Y.K. Sun, B. Scrosati, J. Power Sources 196 (2011) 343–348.
[25] D. Marmorstein, T.H. Yu, K.A. Striebel, F.R. McLarnon, J. Hou, E.J. Cairns, J. Power Sources 89 (2000) 219–226.
[26] M.Y. Chu, Y.S. Nimon, S.J. Visco, WO Patent 2002/41416 A2.
[27] S.J. Visco, Y.S. Nimon, B.D. Katz, US Patent 2011/0039144 A1.
[28] M. Holzapfel, A. Martinent, F. Alloin, B. Le Gorrec, R. Yazami, C. Montella, J. Electroanal. Chem. 546 (2003) 41–50.
[29] A. Martinent, PhD thesis, Institut National Polytechnique de Grenoble, 2001.
[30] J.Y. Song, H.H. Lee, Y.Y. Wang, C.C. Wan, J. Power Sources 111 (2002) 255–267.
[31] B.A. Boukamp, Solid States Ionics 143 (2001) 47–55.
[32] L. Yuan, X. Qiu, L. Chen, W. Zhu, J. Power Sources 189 (2009) 127–132.